CRYSTAL GROWTH & DESIGN

pubs.acs.org/crystal

Article

Single-Crystal Intermetallic Catalysts Using MoS_2 as a Growth Template

Ama D. Agyapong and Suzanne E. Mohney*

Cite This: *Cryst. Growth Des.* 2024, 24, 1578−1590

Read Online

ACCESS | Metrics & More | Article Recommendations | Supporting Information

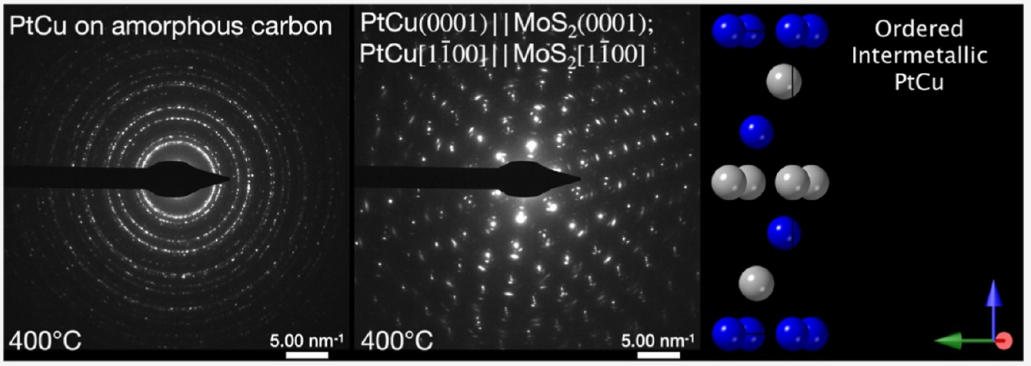

ABSTRACT: Intermetallic alloy phases and especially ordered intermetallic phases offer interesting chemical and physical properties. For example, many ordered intermetallics are attractive catalysts including Pt- and Pd-bearing phases. To better understand and exploit these materials, single crystals offer advantages. Here, we demonstrate the preparation of highly oriented or epitaxial thin films of the intermetallics PdCu, PtCu, PdIn, and $PtAl_2$ on single-crystal MoS_2. We find that cubic PdCu and PtCu films orient on MoS_2 with the epitaxial relationship PdCu (111)||MoS_2 (0001); PdCu[$\bar{2}$11]||MoS_2 [1$\bar{1}$00] when cosputtered at room temperature. However, they are metastable disordered (or random) alloys. Upon annealing at 400 °C, we find evidence for ordering of PtCu. This ordered intermetallic is hexagonal and adopts the orientation PtCu (0001)||MoS_2 (0001); PtCu[1$\bar{1}$00]||MoS_2 [1$\bar{1}$00]. The ordered intermetallic PdIn forms at room temperature with the orientation PdIn (111)||MoS_2 (0001); PdIn[1$\bar{1}$0]||MoS_2 [1$\bar{1}$00]; however, it is a textured film with a wide mosaic spread, even after annealing at 400 °C. The ordered $PtAl_2$ intermetallic phase does not grow epitaxially at room temperature; however, upon annealing at 400 °C, we observe the $PtAl_2$(100) face on MoS_2(0001) rather than the initially expected $PtAl_2$(111) face. The criteria we used previously to predict low-temperature epitaxy of elemental metals remain reliable (high adatom mobility, lack of reactivity with MoS_2, and matching symmetry with the basal plane of MoS_2). However, the presence of an order−disorder transition on the phase diagram, as found for PdCu and PtCu intermetallics, can sometimes promote the formation of a metastable disordered phase at room temperature despite epitaxy on MoS_2.

1. INTRODUCTION

The study of catalysts has primarily focused on metals and alloys since the 1950s; however, there has been a recent increase in publications that examine intermetallic catalysts.[1] Ordered intermetallic phases are multicomponent alloys with each metal on its own crystallographic sublattice. They differ from disordered alloys, in which different metals randomly populate lattice sites (Figure 1).

When certain ordered intermetallic phases are employed as catalysts, they outperform their disordered counterparts, which nevertheless share the same composition.[2] Order can create a catalytic surface that selectively favors specific reactions,[1] leading to high selectivity in chemical transformations such as selective hydrogenation.[3,4] In some ordered intermetallic phases, atoms of a catalytically active element are never the nearest neighbors. In addition, there are fewer possible configurations for nearest neighbors surrounding a catalytic

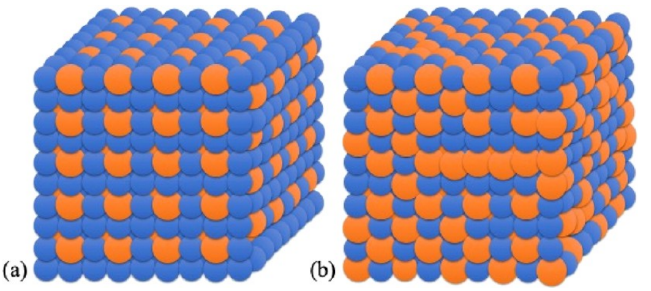

Figure 1. (a) Ordered intermetallic and (b) disordered alloy.

Received: October 1, 2023
Revised: January 14, 2024
Accepted: January 16, 2024
Published: February 6, 2024

element in the ordered alloy. The steric effects resulting from the long-range order in such intermetallic phases play a critical role in this selectivity. Ordered intermetallic crystals have the potential to revolutionize catalytic processes, enabling the achievement of an ideal balance between high activity and selectivity in semihydrogenation,[1] oxidative dehydrogenation,[5] and oxygen reduction reactions.[6]

Because of their promising performance, more studies on intermetallic catalysts are warranted. Existing studies mainly focus on nanoparticles, which can lead to different crystallographic facets participating in the catalytic process.[5,7−10] Furthermore, eliminating grain boundaries reduces the disruption in long-range order, motivating our desire to synthesize single crystals. Single crystal intermetallic films are therefore highly desirable for fundamental surface science studies to observe and understand catalytic mechanisms specific to a particular atomic configuration of an ordered intermetallic surface.

Obtaining ordered intermetallic phases with a high phase purity can be challenging. In some cases, other phases can be present due to slight variations in a sample's composition or metastability of a related disordered phase, resulting in different catalytic properties than intended. Grain boundaries also represent local disruptions to the atomic order. Thus, there is a need for a process that can produce intermetallic catalysts with high phase purity and few or no grain boundaries−single crystals.

While the discovery of graphene opened the gateway to fascinating properties of two-dimensional semiconductors,[11] it is the van der Waals nature of these 2D layered materials that may also provide an approach to growing ordered alloy phases. 2D layered materials have strong covalent bonds within the layers and weak van der Waals interlayer bonds. The van de Waals bonds can be broken easily by mechanical,[12−14] liquid,[15] or chemical[16,17] exfoliation to isolate single to few layers, resulting in atomically flat and potentially inert surfaces ideal for epitaxial film growth. Past studies observed room-temperature epitaxy of elemental metals with ≥20% lattice mismatch on MoS_2[18] and WSe_2.[19] Epitaxy was attributed to a match of the crystallographic symmetry, thermodynamic stability, and high metal atom mobilities on the TMD surfaces. The criteria for achieving metal quasi-van der Waals epitaxy on TMDs require that (1) the metals have a crystallographic plane with an arrangement of atoms with symmetry to match that of the basal plane of the TMD, e.g., hexagonally arranged atoms on the (111) plane of face-centered cubic (FCC) or the (0001) plane of hexagonally close-packed (HCP) crystals, (2) the metal atoms have a low energy barrier to diffusion on the TMD surface (≤0.60 eV), and (3) the metal/TMD interfaces are free of interfacial reactions.

In this study, we explore the possibility that this discovery can be taken a step further and exploited for the synthesis of single-crystal-ordered intermetallic alloys or phases. We prepare intermetallic alloys with high phase purity on MoS_2 as a growth template. We apply the guidelines from previous work on quasi-van der Waals epitaxy of metals on TMDs to new work on ordered intermetallic alloys on TMDs and expand our understanding of how metal/TMD interactions affect heteroepitaxy. Specifically, we deposit PdCu, PtCu, PdIn, and $PtAl_2$ alloys on MoS_2 using exfoliated flakes for this demonstration and investigate the resulting structures.

2. METHODOLOGY

2.1. Criteria for Quasi-van der Waals Epitaxy. We began by checking the criteria for quasi-van der Waals epitaxy between the selected intermetallic phases and MoS_2 using the guidelines presented in prior studies on room-temperature epitaxy of metals on TMDs.[18,19] We chose Pd- and Pt-based ordered intermetallics because Pd and Pt are common but expensive catalysts.[5,6,20−22] The intermetallic phases with a plane of hexagonally arranged atoms may orient with the basal plane of MoS_2 provided they are thermodynamically stable against the reaction with MoS_2, and the atoms have adequate atomic mobilities on the surface of MoS_2. The atomic arrangements of these ordered alloys on MoS_2 can be visualized by obtaining the crystallographic information file (CIF) from the Materials Project Database[23] and orienting the crystals using the CrystalMaker software.

Figure 2 shows the hexagonally arranged sulfur atoms on the basal plane of MoS_2 and the different crystal structures of the intermetallic phases of interest. Table 1 lists the crystallographic information[24−27] for the different intermetallics along with their repeat distance with respect to the basal plane of MoS_2 and their lattice mismatch. The CuPt prototype has atoms in a hexagonal arrangement on the (0001) plane like MoS_2. Compounds with CaF_2 and CsCl structures have atoms in a hexagonal arrangement on the (111) plane. By obtaining the geometric relationships between the atomic positions of the intermetallics with respect to the sulfur−sulfur distance on the (0001) plane of MoS_2, we were able to calculate the lattice mismatch for the predicted hexagonal (0001) or the cubic (111) planes of the intermetallics on the basal plane of MoS_2. The calculated lattice mismatch ranges from −31.2 to 1.0%, where for $PtAl_2$, we matched two unit cells of MoS_2 to one of

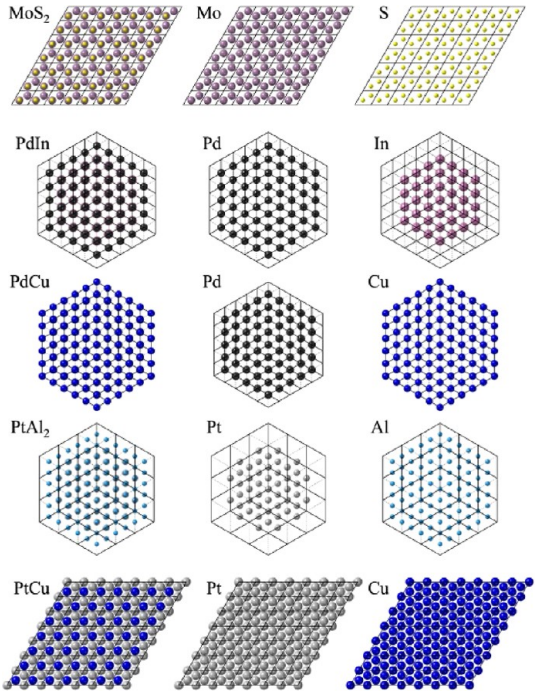

Figure 2. Basal plane of MoS_2 and the PdIn (111), PdCu (111), $PtAl_2$ (111), and PtCu (0001) planes with hexagonal arrangements of atoms. The first column displays a projection of both elements. The second column displays only Mo or the catalytic component. The third column displays only S or secondary metals.

https://doi.org/10.1021/acs.cgd.3c01167
Cryst. Growth Des. 2024, 24, 1578−1590

Table 1. Crystallographic Information for MoS_2 and Intermetallic Phases of Interest[a]

alloys	proto-type	Bravais lattice	a (nm)	c (nm)	plane	repeat distance formula	repeat distance	number of MoS_2 cells	lattice mismatch
MoS_2	MoS_2	hexagonal	0.316	1.230	0001	a	0.316		
$PtAl_2$	CaF_2	cubic	0.591		111	2a	0.836	2	−6.44%
PdCu	CsCl	cubic	0.298		111	2a	0.421	1	−25.0%
PtCu	CuPt	hexagonal	0.313	1.498	0001	a	0.313	1	1.0%
PdIn	CsCl	cubic	0.325		111	2a	0.460	1	−31.2%

[a]Lattice parameters obtained from the ASM Alloyed Phase Diagram Database.[24−27]

$PtAl_2$. Although some mismatch values are high, they might not be a limiting factor for achieving epitaxy on MoS_2, since large lattice mismatches have been reported for successful van der Waals epitaxy of many metals on TMDs.[18,19]

Next, we examined the diffusion barriers (Table 2) of adatoms on the basal plane of MoS_2 for the elemental components of the intermetallic phases of interest from density functional theory (DFT) calculations by Saidi.[28] The atoms we have chosen have relatively low diffusion barriers ranging from 0.15−0.60 eV on MoS_2. Many elemental metals like these with low diffusion barriers have been found to be epitaxial on MoS_2, even when deposited at room temperature (or annealed at ∼400 °C), while metals with diffusion barriers greater than 0.85 eV (i.e., Ni and Ru) were not epitaxial.[18] Thus, we expect that atomic components of the selected intermetallics could have adequate atomic mobility for ordering on the MoS_2 surface.

Table 2. Surface Diffusion Barriers of Metal Atoms on MoS_2 Obtained from Saidi (2015)[28]

metals	diffusion barrier (eV)
Al	0.28
Cu	0.33
Pd	0.43
In	0.15
Pt	0.60

Finally, we looked at the literature to obtain information about the reactivity between the metals in the intermetallic phases and MoS_2. Calculated ternary phase diagrams at 25 °C for Cu, Pd, and Pt show lack of reactivity with MoS_2.[29] Therefore, the ordering of PtCu and PdCu on the MoS_2 surface should not be limited by interfacial reactions at modest temperatures. Although we could not find ternary phase diagrams for the Al−Mo−S system, we did find studies that reported on the reactivity of these systems. Aluminum films have been reported via a selected area electron diffraction (SAED) pattern to be epitaxial on exfoliated MoS_2 when deposited at room temperature and after annealing at 400 °C.[18] Therefore, we do not expect a reaction between Al and MoS_2 at modest temperatures to be a limiting factor for the epitaxy of $PtAl_2$.

2.2. Experimental Procedure. To study the growth of films on MoS_2, we prepared plan-view samples for transmission electron microscopy (TEM) and electron diffraction. Bulk MoS_2 crystals received from the 2D Crystal Consortium at Penn State were mechanically exfoliated by using the Scotch-tape method directly on Quantifoil gold TEM grids. The Quantifoil grids are covered by amorphous carbon, making it possible to examine differences in the crystallographic orientation of our films on an amorphous support compared to crystalline MoS_2 flakes. Each intermetallic alloy was then cosputtered by DC magnetron sputtering directly onto exfoliated MoS_2 at a base chamber pressure of 2×10^{-7} Torr and a working pressure of 5 mTorr with Ar gas. In order to deposit films of the desired composition, we first calibrated the deposition rate of each, and then we calculated the ratio of thickness (Table 3) of each element needed based on the composition and atomic densities of phases from the ASM Alloy Phase Diagram Database.[24−27] In some cases, we adjusted the cosputtering rates if we did not achieve the desired phase on the first attempt. A total thickness of 25−30 nm was deposited to keep the films electron-transparent for TEM, and the films were continuous or nearly continuous. Plan-view TEM micrographs are provided in Figures S1−S4 in the Supporting Information. The alloys were cosputtered at a deposition rate of 0.2−0.3 Å/s and annealed in a rapid thermal annealing (RTA) furnace at 400 °C for 5 min in an Ar environment.

Table 3. Target Thicknesses of Elements in the Intermetallic Alloys

alloy	active metal (nm)	secondary metal (nm)
$PtAl_2$	9	21
PdCu	15	15
PtCu	18	12
PdIn	12	18

The intermetallic films on exfoliated MoS_2 were characterized by TEM using an FEI Talos F200X system at an accelerating voltage of 200 kV to obtain plan-view TEM images, SAED patterns, and energy dispersive spectroscopy (EDS) maps. The TEM, SAED, and EDS data provide us with the crystallinity, morphology, phase, orientation, and composition of the intermetallic phases.

3. RESULTS AND DISCUSSION

3.1. PdCu. Figure 3 shows the electron diffraction pattern for as-deposited PdCu on MoS_2. According to EDS, its composition was approximately 52 at. % Pd and 48 at. % Cu, and the film was continuous (Figure S1). The pattern shows spots from the MoS_2 flake and spots or narrow arcs from the PdCu film, as well as reflections from double diffraction. We find the PdCu (111) plane to be aligned with the basal plane of the MoS_2 surface with the PdCu $[\bar{2}11]$ and MoS_2 $[1\bar{1}00]$ directions aligned. After annealing the sample at 400 °C, we found that the PdCu film exhibits the same orientational relationship on the MoS_2 surface over different areas (Figure 4).

In the Cu−Pd system, there is an ordered PdCu phase at room temperature with the CsCl crystal structure ($Pm\bar{3}m$) with a wide range of homogeneities, but at higher temperatures, there is a disordered FCC phase belonging to the $Fm\bar{3}m$ space group. The highest temperature the ordered

https://doi.org/10.1021/acs.cgd.3c01167
Cryst. Growth Des. 2024, 24, 1578−1590

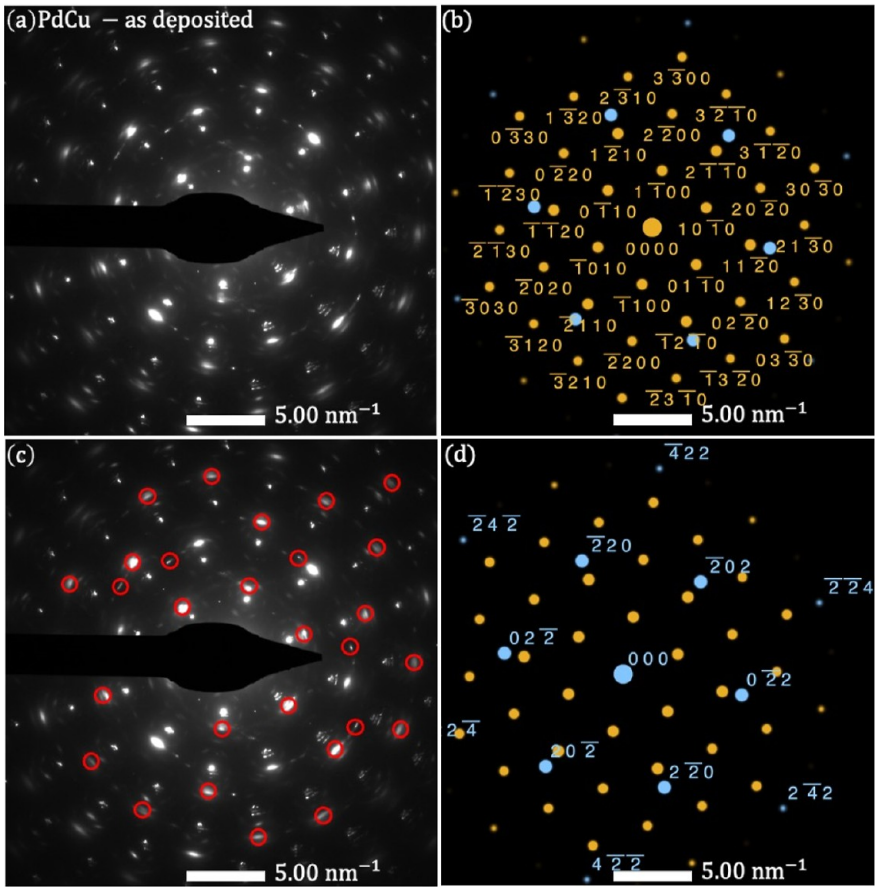

Figure 3. SAED pattern of the disordered PdCu phase on MoS_2 (a) for the as-deposited condition and (b) simulated primary diffraction spots for the [111] zone axis of disordered PdCu overlaid with the [0001] zone axis of MoS_2 with only the MoS_2 spots labeled. The orientation relationship is PdCu (111)||MoS_2 (0001); PdCu[$\bar{2}$11]||MoS_2 [1$\bar{1}$00]. (c) SAED pattern identifying double diffraction (circled spots). (d) Simulated diffraction spots of the [111] zone axis of disordered PdCu (labeled) overlaid with the [0001] zone axis of MoS_2 (not labeled).

phase is stable is at 598 °C,[24] at which the ordered phase is rich in Cu. To determine whether we achieved ordering in addition to epitaxy, we compared experimental SAED patterns with simulated patterns of both the disordered and ordered PdCu phases. We find that the PdCu phase is disordered, with *d*-spacings most closely matching the reference pattern for the disordered PdCu phase. The 0$\bar{1}$0 reflections that correspond to the ordered Pm$\bar{3}$m phase were missing from the SAED pattern (Figure 5). The measured *d*-spacings were also much closer to the *d*-spacings of the disordered PdCu phase, leading us to conclude that the phase formed on exfoliated MoS_2 was disordered PdCu both for the as-deposited case and after annealing. Additional spots are present in the patterns due to double diffraction. There are faint double spots (up to six) around bright reflections as well as additional spots that we confirm are from double diffraction by displacing the origin of the pattern for MoS_2 onto the PdCu $\bar{2}$20, $\bar{2}$02, 0$\bar{2}\bar{2}$, 2$\bar{2}$0, 20$\bar{2}$, and 02$\bar{2}$ reflections. We also compared SAED patterns with rings from polycrystalline PdCu acquired from the areas of the sample without MoS_2 to simulated ordered and disordered PdCu patterns (not shown) and found that our experimental data again corresponded to the disordered phase for both the as-deposited and the annealed cases.

We were able to form only the disordered phase of PdCu even after annealing at 400 °C for 5 min, even though EDS showed a composition of 51 at. % Pd and 49 at. % Cu for the annealed film, within the range of homogeneity for the ordered phase. Similar observations have been made for the CoPt intermetallic phase (on other substrates), where the ordered phase was formed only when the films were annealed at 600 or 700 °C,[30] close to the transition temperature (825 °C).[31] It is possible that our annealing temperature was too low to form ordered PdCu due to kinetic limitations. However, annealing at temperatures higher than 400 °C could possibly lead to degradation of the MoS_2 flake, and we did not pursue annealing at higher temperatures.

3.2. PtCu. Similar to the Pd−Cu system, the Pt−Cu system also has an ordered R$\bar{3}$m phase at room temperature with a wide composition range of 43−76 at. % Pt at room temperature[25] and a disordered Fm$\bar{3}$m phase at higher temperatures (above 830 °C near the equiatomic composition). According to EDS, the films were Pt-rich, with 70 at. % Pt and 30 at. % Cu but within the single-phase region. Some cracks were present in the otherwise continuous films (Figure S2). Both the FCC and HCP phases are predicted to orient on the basal plane of MoS_2. The diffraction spots for the [0001] zone axis of the ordered R$\bar{3}$m phase and the [111] zone axis for the disordered Fm$\bar{3}$m phase of PtCu are similar, with a very small difference in the *d*-spacing as observed in overlapping simulated diffraction patterns of the two phases (Figure 6a), making it hard to distinguish between the two phases with *d*-spacing measurements alone. Although the measured *d*-spacing and the ratios of distances from the origin of the MoS_2 and neighboring PtCu diffraction spots for the experimental SAED

https://doi.org/10.1021/acs.cgd.3c01167
Cryst. Growth Des. 2024, 24, 1578−1590

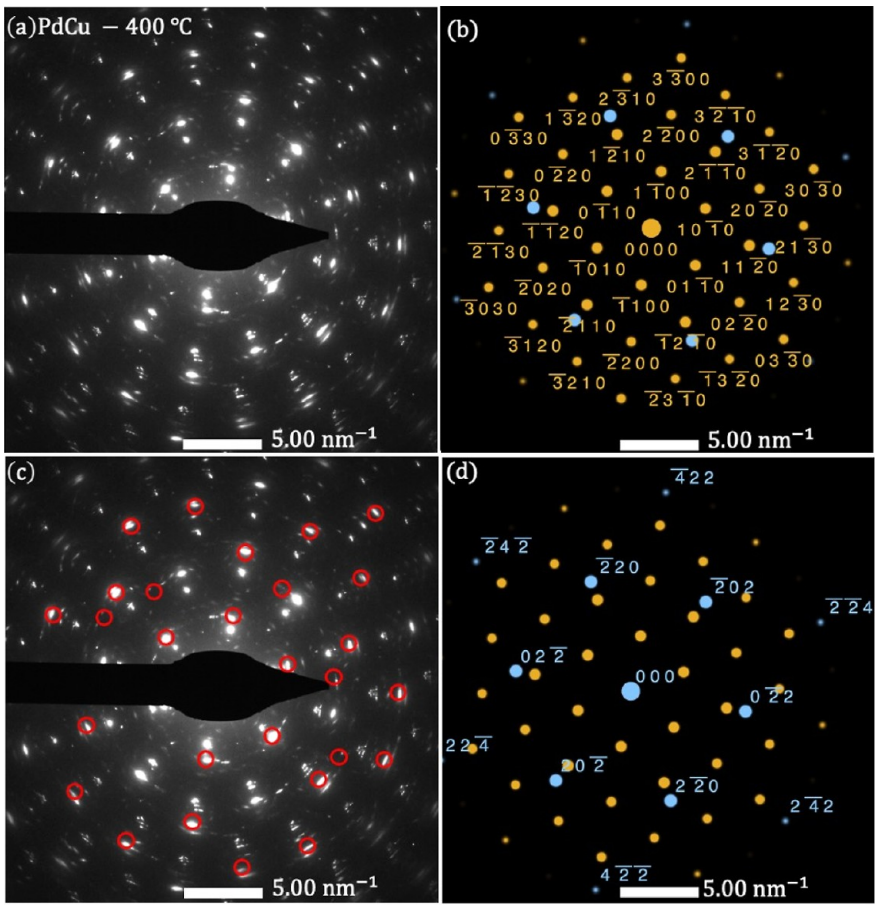

Figure 4. SAED pattern of the disordered PdCu phase on MoS_2 (a) for the annealed (400 °C) condition and (b) simulated primary diffraction spots for the [111] zone axis of disordered PdCu overlaid with the [0001] zone axis of MoS_2 with only the MoS_2 spots labeled. The orientation relationship is PdCu (111)||MoS_2 (0001); PdCu[$\bar{2}$11]||MoS_2 [1$\bar{1}$00]. (c) SAED pattern identifying double diffraction (circled spots). (d) Simulated diffraction spots of the [111] zone axis of disordered PdCu (labeled) overlaid with the [0001] zone axis of MoS_2 (not labeled).

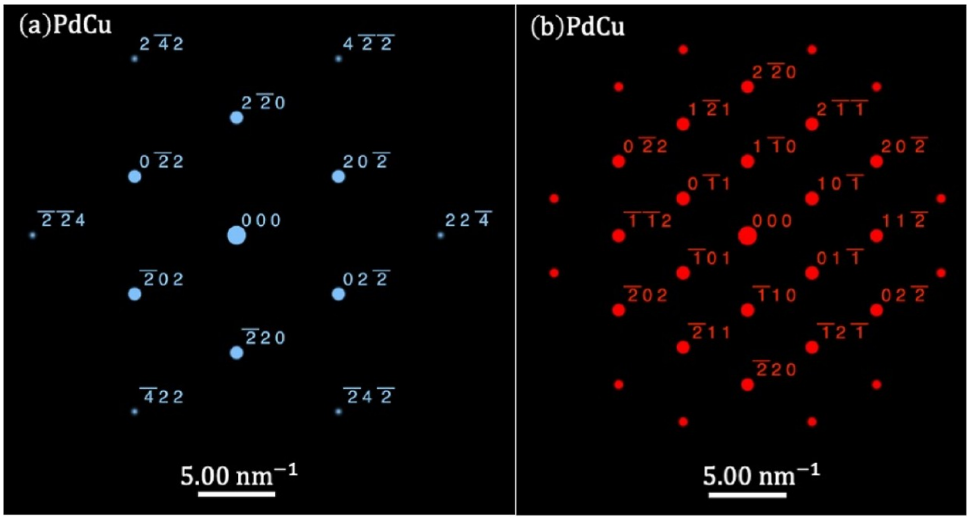

Figure 5. Simulated diffraction patterns of the [111] zone axis of (a) disordered and (b) ordered PdCu.

pattern closely matched the ordered PtCu phase, we were unable to conclusively determine that we formed an ordered PtCu phase. However, we collected SAED patterns from areas of the film on amorphous carbon without exfoliated MoS_2, where the film was polycrystalline and exhibited rings rather than spots in the SAED patterns for the as-deposited and annealed conditions (Figure 6b,c). Although the as-deposited SAED polycrystalline rings correspond to the referenced polycrystalline rings for the disordered PtCu phase (Figure 6b), we observed additional rings in the annealed SAED polycrystalline pattern consistent with the ordered PtCu phase (Figure 6c), most notably the 0003 reflection near the origin

https://doi.org/10.1021/acs.cgd.3c01167
Cryst. Growth Des. 2024, 24, 1578−1590

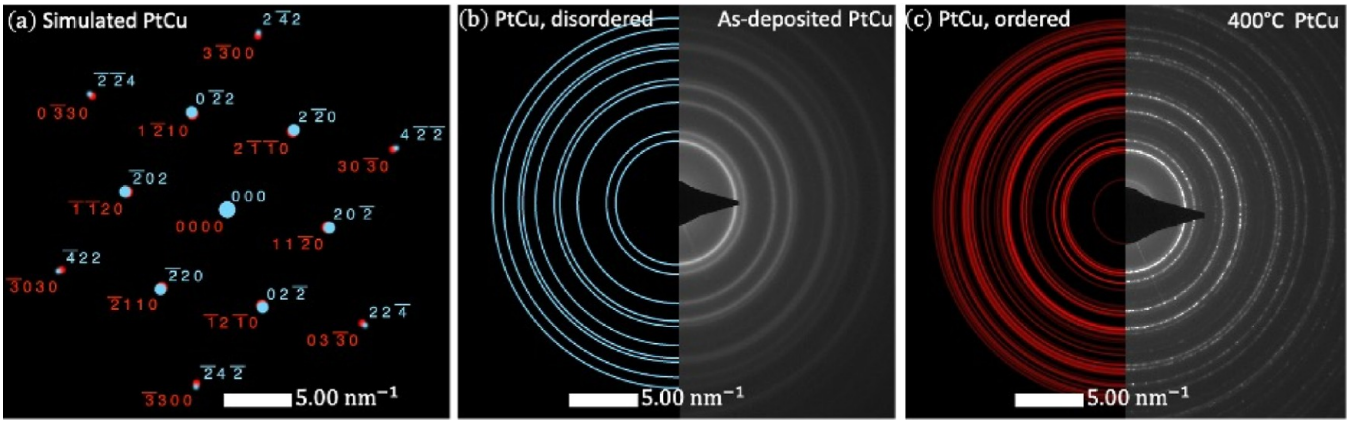

Figure 6. (a) Simulated diffraction pattern of ordered and disordered PtCu. The disordered pattern is indicated by Miller–Bravais indices (*hkl*), and the ordered pattern is indicated by the Miller–Bravais (*hkil*) indices. (b) SAED pattern of as-deposited PtCu (right) and simulated polycrystalline rings for disordered PtCu (left). (c) SAED pattern of annealed PtCu (right) and simulated polycrystalline rings for ordered PtCu annealed (left). The SAED patterns were obtained from the areas of the sample without MoS_2.

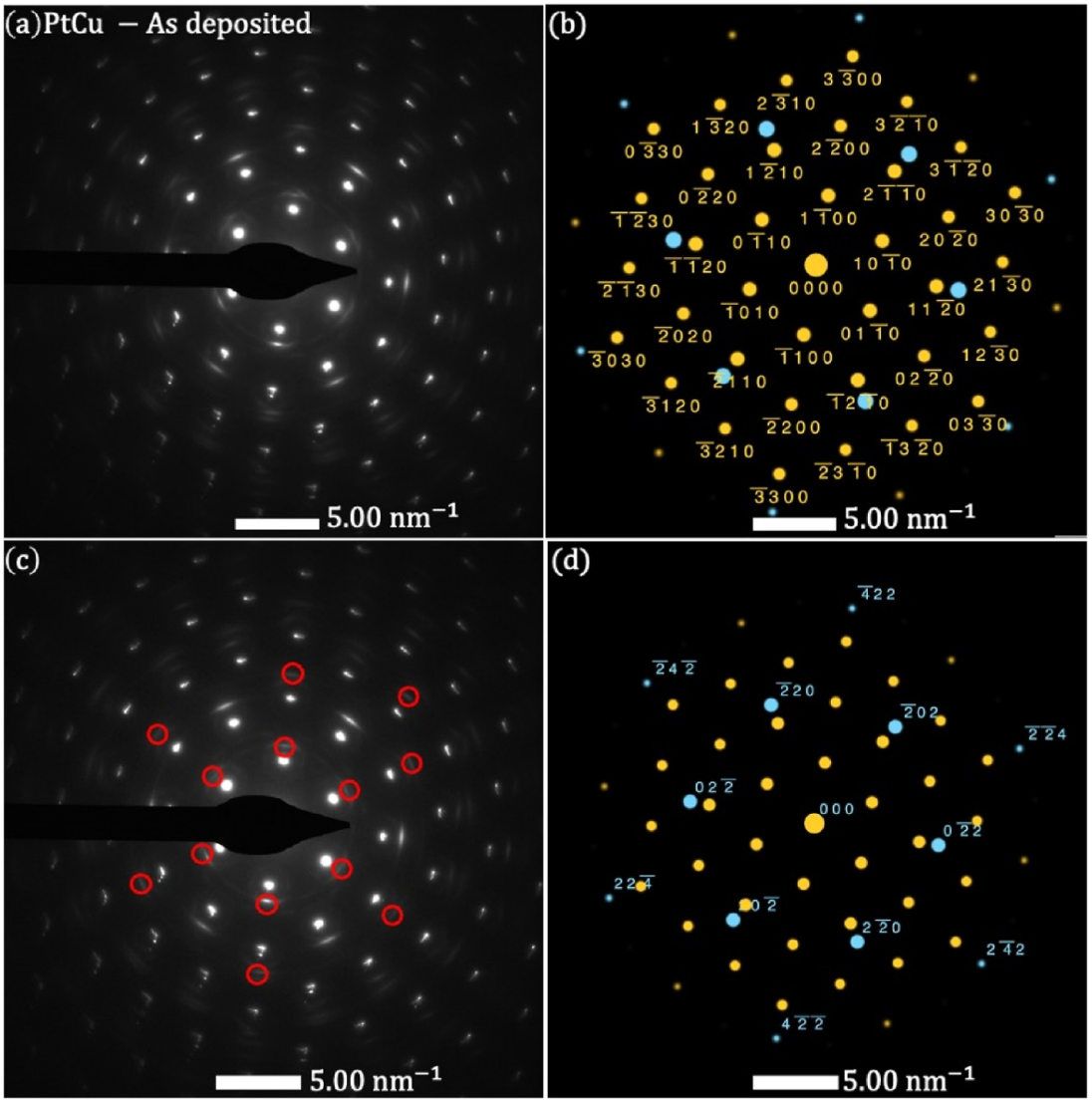

Figure 7. SAED pattern of the disordered PtCu phase on MoS_2 (a) as-deposited and (b) simulated diffraction spots of the [111] zone axis of PtCu overlaid with the [0001] zone axis of MoS_2 with the MoS_2 spots labeled. The orientation relationship is PtCu (111)||MoS_2 (0001); PtCu[$\bar{2}11$]|| MoS_2 [$1\bar{1}00$]. (c) SAED pattern showing double diffraction events circled. (d) Simulated diffraction spots of the [111] zone axis of PtCu (labeled) overlaid with the [0001] zone axis of MoS_2.

https://doi.org/10.1021/acs.cgd.3c01167
Cryst. Growth Des. 2024, 24, 1578–1590

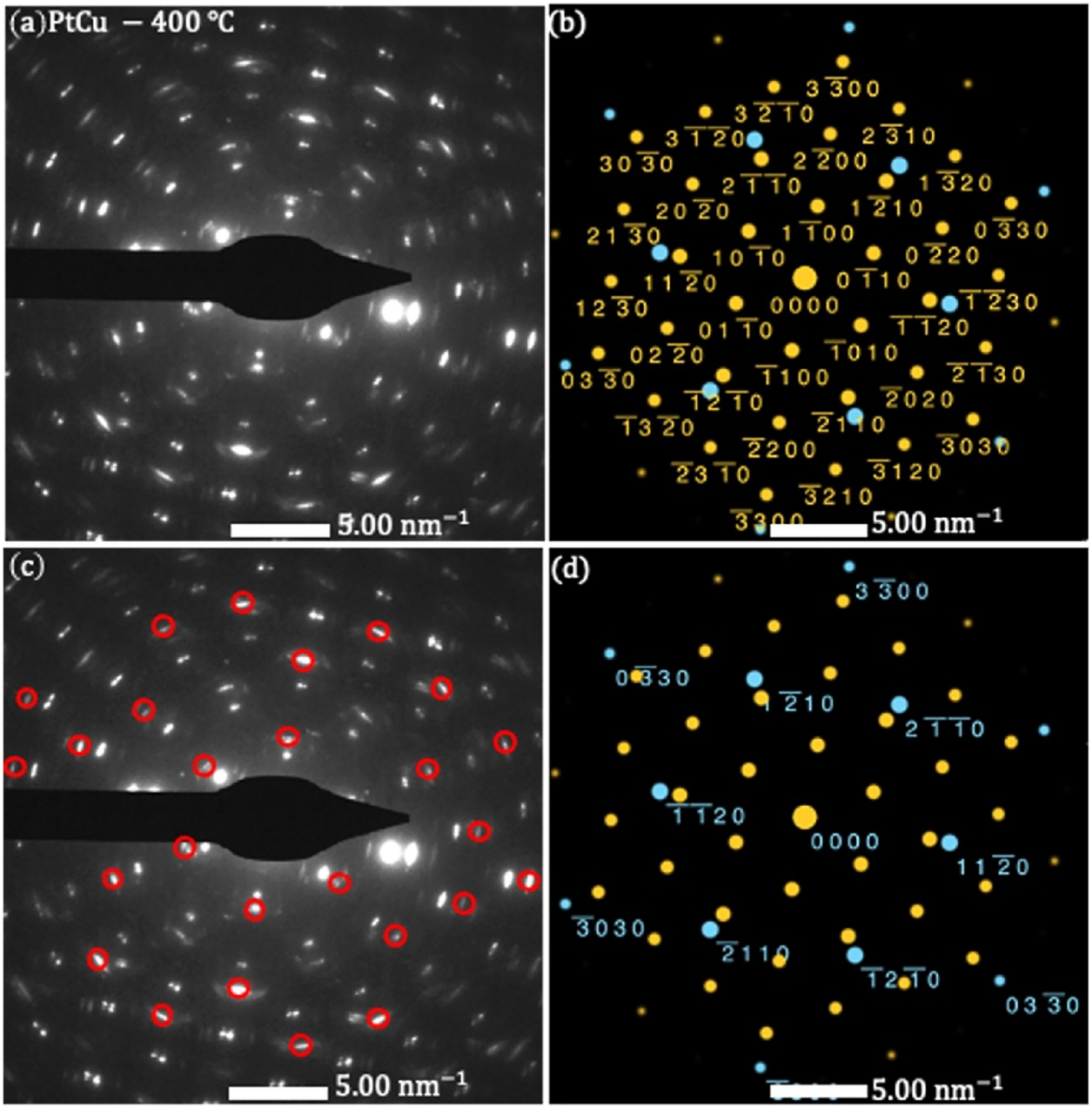

Figure 8. SAED pattern of the ordered PtCu phase on MoS_2 (a) annealed at 400 °C and (b) simulated diffraction spots of the [0001] zone axis of PtCu overlaid with the [0001] zone axis of MoS_2 with the MoS_2 spots labeled. The orientation relationship is PtCu (0001)||MoS_2 (0001); PtCu[1$\bar{1}$00]||MoS_2 [1$\bar{1}$00]. (c) SAED pattern showing double diffraction events circled. (d) Simulated diffraction spots of the [0001] zone axis of PtCu (labeled) overlaid with the [0001] zone axis of MoS_2.

but also many other faint rings for ordered PtCu. Hence, PtCu exhibits at least some degree of ordering after it is annealed at 400 °C.

The diffraction patterns for as-deposited PtCu/MoS_2 (Figure 7) show spots from MoS_2 and bright arcs from PtCu. The orientation relationship is PtCu (111)||MoS_2 (0001); PtCu[$\bar{2}$11]||MoS_2 [1$\bar{1}$00]. The arcs indicate that the PtCu film is textured and oriented. After annealing at 400 °C, we see clear bright spots for both the PtCu and MoS_2, indicating improved alignment of PtCu after annealing (Figure 8). The orientation is PtCu (0001)||MoS_2 (0001); PtCu[1$\bar{1}$00]||MoS_2 [1$\bar{1}$00]. We also observed additional arcs from double diffraction of MoS_2 and PtCu.

3.3. PdIn. The PdIn films were continuous (Figure S3), with EDS indicating a composition of 53 at. % Pd and 47% at. % In. After annealing, the composition was 55 at. % Pd and 45 at. % In, possibly due to evaporation of In. Both compositions are within the range of homogeneity of PdIn. The SAED patterns for the as-deposited (Figure 9) and annealed (Figure 10) PdIn indicate that the intermetallic phase is highly textured and orients on the MoS_2 substrate. The orientation relationship is PdIn (111)||MoS_2 (0001); PdIn[1$\bar{1}$0]||MoS_2 [1$\bar{1}$00] in both the as-deposited and the annealed cases. Some arcs correlate to the textured PdIn [111] zone axis, and others correspond with double diffraction between PdIn and MoS_2. We found all spots associated with the ordered PdIn phase, with the exception of the $\bar{1}2\bar{1}$ reflection family, which has

https://doi.org/10.1021/acs.cgd.3c01167
Cryst. Growth Des. 2024, 24, 1578−1590

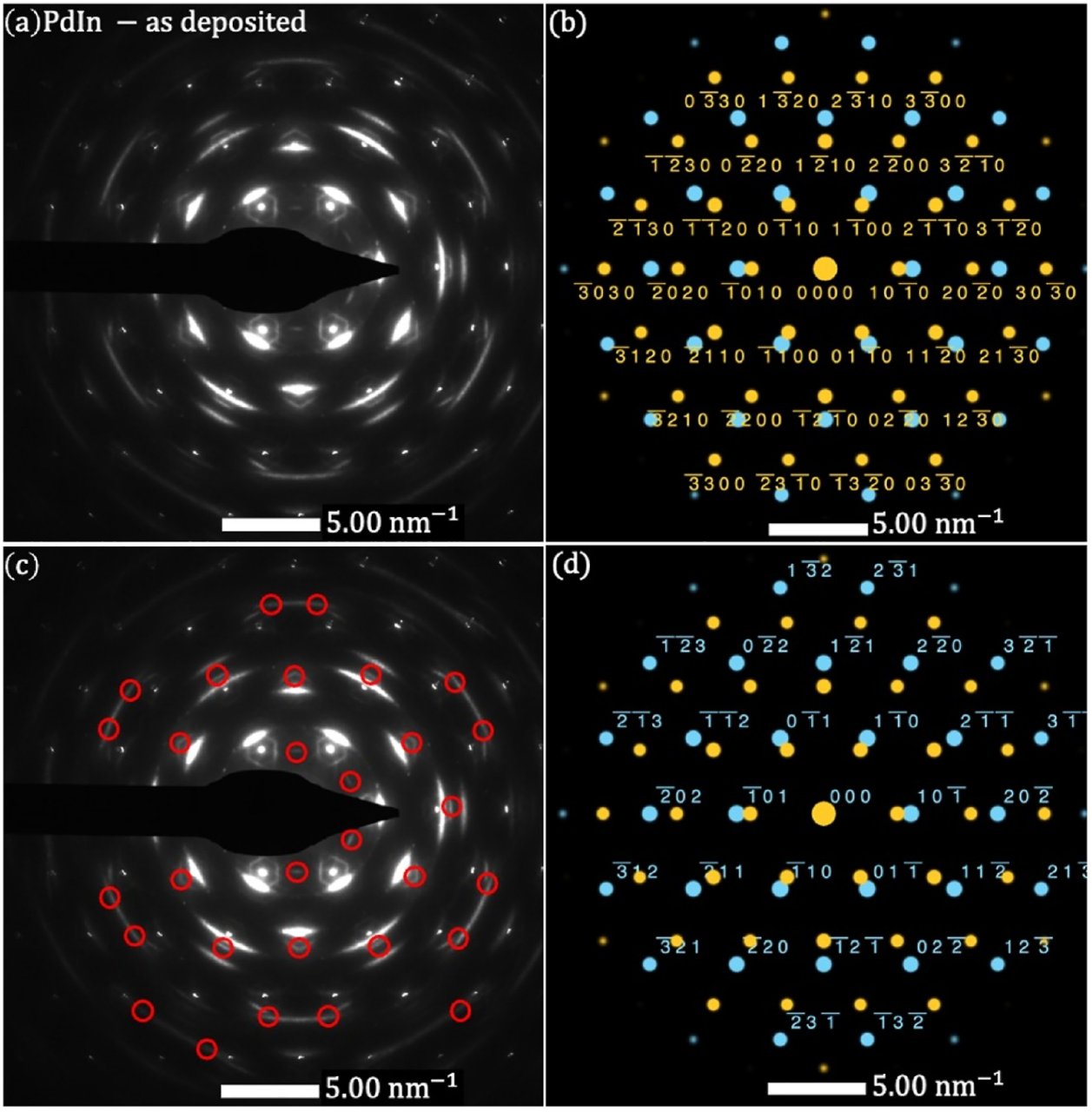

Figure 9. SAED pattern of the PdIn on MoS_2 (a) for the as-deposited condition and (b) simulated diffraction spots of the [111] zone axis of PdIn overlaid with the [0001] zone axis of MoS_2 with the MoS_2 spots labeled. The orientation relationship is PdIn (111)||MoS_2 (0001); PdIn[1$\bar{1}$0]||MoS_2 [1$\bar{1}$00]. (c) SAED pattern showing double diffraction events circled. (d) Simulated diffraction spots of the [111] zone axis of PdIn (labeled) overlaid with the [0001] zone axis of MoS_2.

weaker intensity in the simulated pattern and is far from the origin. We see double diffraction of MoS_2 in the form of lines forming a hexagon around the MoS_2 spots and additional faint spots that are due to regions of slightly differing orientation of MoS_2 (Figures 9c and 10c). Double diffraction patterns were also generated. Spots corresponding to the PdIn [111] zone axis were superimposed with the origin of the PdIn [111] zone axis patterns at the 1$\bar{2}$10, 2$\bar{1}\bar{1}$0, 11$\bar{2}$0, $\bar{1}$2$\bar{1}$0, $\bar{2}$110, and $\bar{1}\bar{1}$20 MoS_2 reflections.

3.4. $PtAl_2$. Films with a composition very near to that of $PtAl_2$ (65 at. % Pt and 35 at. % Al according to EDS) were very nearly continuous (Figure S4). All spots observed in the SAED pattern for the as-deposited $PtAl_2$ sample belong to the MoS_2 basal plane (Figure 11a). The SAED pattern also shows a single ring that corresponds to the 220 reflection of polycrystalline $PtAl_2$ (Figure 11b). We collected SAED patterns from areas without MoS_2 (Figure 11c), which confirmed the $PtAl_2$ phase with rings corresponding to the 111, 220, and 331 reflections. We observed alignment of the $PtAl_2$ film on MoS_2 after annealing at 400 °C (Figure 12). Unlike our prediction, the $PtAl_2$ (100) plane grew on (0001) MoS_2 instead of the originally expected (111) plane. The orientation relationship for the annealed $PtAl_2$ on MoS_2 is $PtAl_2$ (100)||MoS_2 (0001); $PtAl_2$ [0$\bar{2}$0]||MoS_2 [2$\bar{1}\bar{3}$0] with a slight rotation of the $PtAl_2$ by approximately 2°, where the [2$\bar{1}\bar{3}$0]direction is perpendicular to the (10$\bar{1}$0) plane. While the calculated lattice mismatch between the basal plane of the MoS_2 and the (111) plane of $PtAl_2$ is −6.4% (Table 1), the

https://doi.org/10.1021/acs.cgd.3c01167
Cryst. Growth Des. 2024, 24, 1578−1590

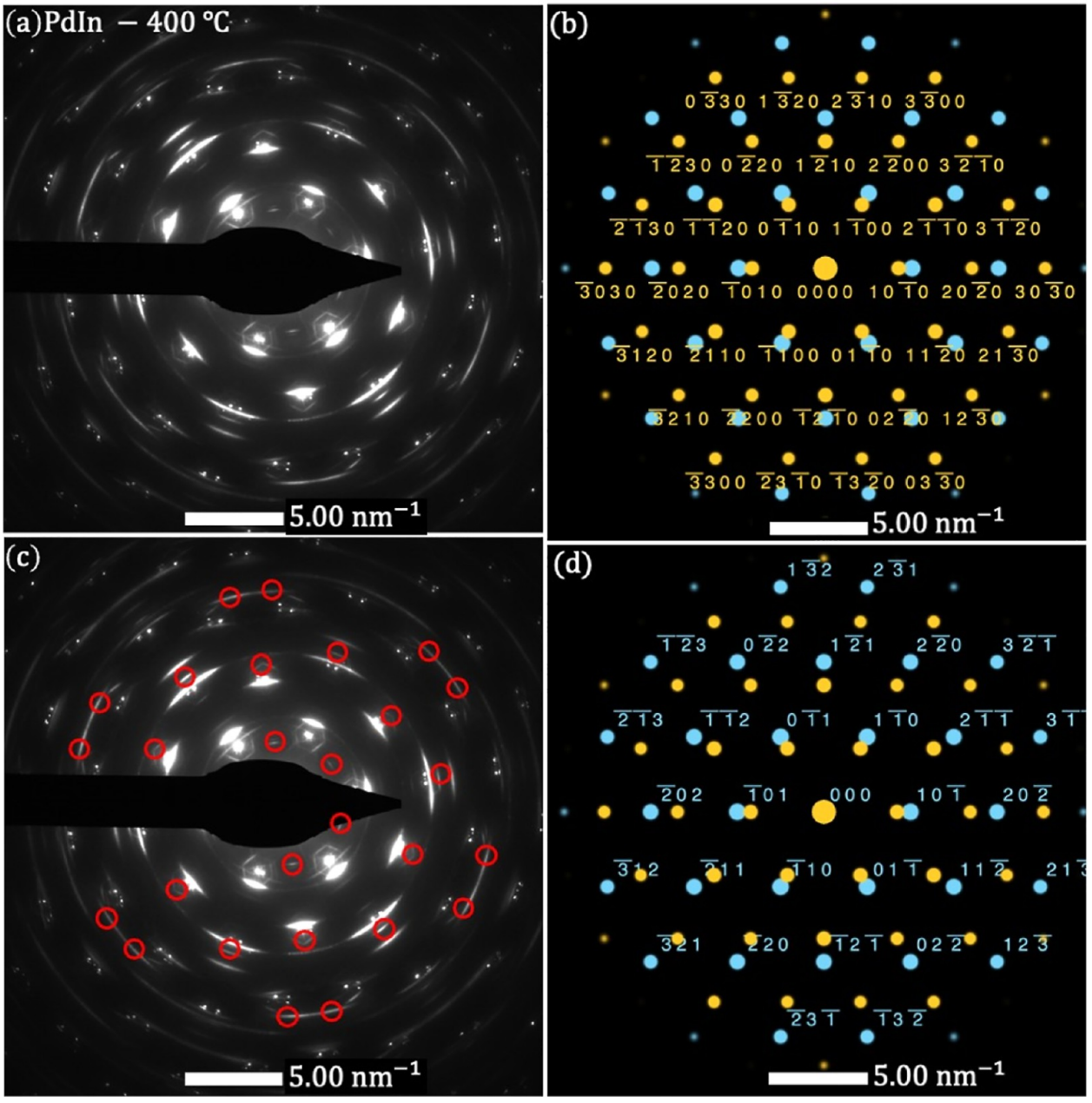

Figure 10. SAED pattern of PdIn on MoS_2 (a) for the annealed condition (400 °C) and (b) simulated diffraction spots of the [111] zone axis of PdIn overlaid with the [0001] zone axis of MoS_2 and the MoS_2 spots labeled. The orientation relationship is PdIn (111)||MoS_2 (0001); PdIn[1$\bar{1}$0]|| MoS_2 [1$\bar{1}$00]. (c) SAED pattern showing double diffraction events circled. (d) Simulated diffraction spots of the [111] zone axis of PdIn (labeled) overlaid with the [0001] zone axis of MoS_2.

(100) plane has two lattice mismatches along the [001] and [010] directions. The lattice mismatch between the (100) plane of $PtAl_2$ and the basal plane of MoS_2 is calculated to be −7.4% and 6.9% along the [001] and [010] directions, respectively. The magnitudes of the lattice mismatches for the (100) plane of $PtAl_2$ are barely larger than the lattice mismatch for the (111) plane (−6.4%), so in retrospect, this orientation relationship is not so surprising.

3.5. Trends in Epitaxy and Ordering. By comparing different materials, we are able to recognize some trends in the epitaxy of intermetallics on single-crystal MoS_2 as well as trends in whether ordered or disordered intermetallic phases form. Although polycrystalline films formed whenever we cosputtered intermetallics at room temperature on amorphous carbon, when the films were deposited on exfoliated (0001) MoS_2, we often observed spot patterns. PdCu, PtCu, and PdIn were all highly oriented or epitaxial as deposited, with easily predicted orientation relationships, while $PtAl_2$ was epitaxial only after annealing in Ar at 400 °C for 5 min. Although we do not know why cubic $PtAl_2$ oriented with the (100) face instead of the (111) face on (0001) MoS_2, we point out that the lattice mismatch was similar, and we suggest that coincidence lattices can be important in quasi-van der Waals epitaxy.

In our prior work with elemental metals, lower barriers predicted by DFT for adatom diffusion on the basal plane of MoS_2 promoted epitaxy, as long as epitaxy was also favored by the crystallography. The barrier for the diffusion of Pt on MoS_2 is higher than that of Cu, Pd, and Al,[18] which may be part of

https://doi.org/10.1021/acs.cgd.3c01167
Cryst. Growth Des. 2024, 24, 1578−1590

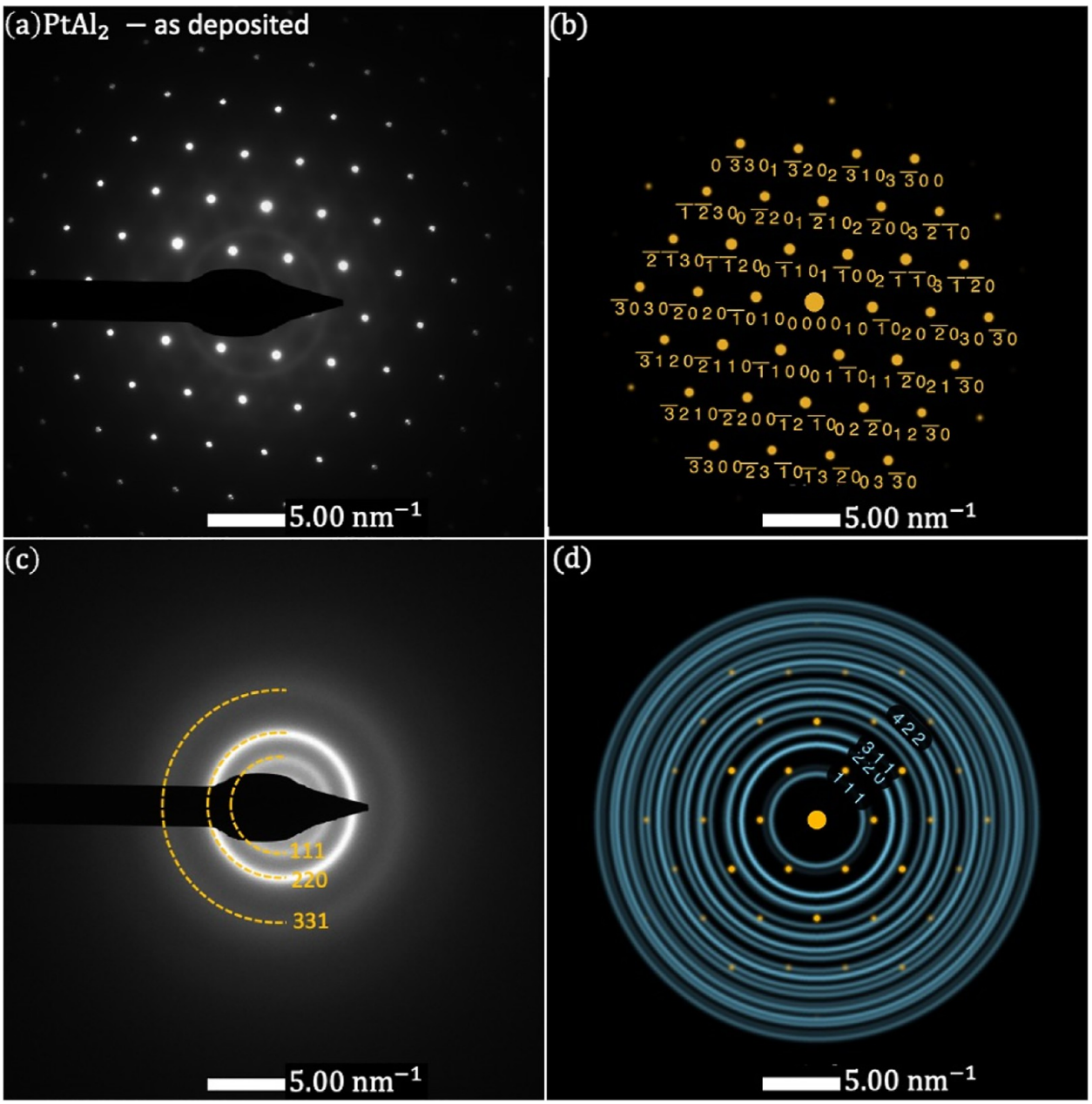

Figure 11. SAED pattern of $PtAl_2$ on MoS_2 (a) for the as-deposited condition collected with the 200 mm selected area aperture and (b) with simulated MoS_2 spots labeled. (c) SAED polycrystalline pattern collected from an area without the presence of the MoS_2 flake showing rings corresponding to the $PtAl_2$ the 111, 220, and 331 reflections. (d) Simulated diffraction spots of the [0001] zone axis of MoS_2 overlaid with polycrystalline $PtAl_2$ rings.

the reason $PtAl_2$ was not epitaxial until after annealing. However, disordered PtCu grew epitaxially. We then consider that diffusion in an ordered intermetallic also requires atoms to remain on their respective sublattices, which logically would be accompanied by a higher barrier to diffusion than that in a disordered crystal. Therefore, the somewhat higher barrier to adatom diffusion of Pt on MoS_2, combined with the lack of a metastable disordered phase of the same composition, may have both contributed to the lack of room-temperature epitaxy of $PtAl_2$

PdCu and PtCu differ from PdIn and $PtAl_2$ in that they are ordered only at lower temperatures. At higher temperatures, a disordered phase without separate sublattices for Pd or Pt atoms becomes stable. PdCu and PtCu were both disordered (but epitaxial) on MoS_2 as deposited, but only PtCu became ordered upon annealing. Neither were at their perfect stoichiometric composition, but annealed PtCu was much further from the perfect 1:1 stoichiometry at 70 atom % Pt compared to PdCu at 51 at. % Pd. The PtCu phase has a particularly wide range of homogeneity (43−76 at. % Pt at room temperature[25]), which means that there are many constitutional point defects. These defects could make diffusion easier. We therefore speculate that a nonstoichiometric composition may have aided the ordering of PtCu at 400 °C, although nonstoichiometry would be unfavorable in catalysts in cases when the ordered nature of an intermetallic improves performance. We also note that deposition with the

https://doi.org/10.1021/acs.cgd.3c01167
Cryst. Growth Des. 2024, 24, 1578−1590

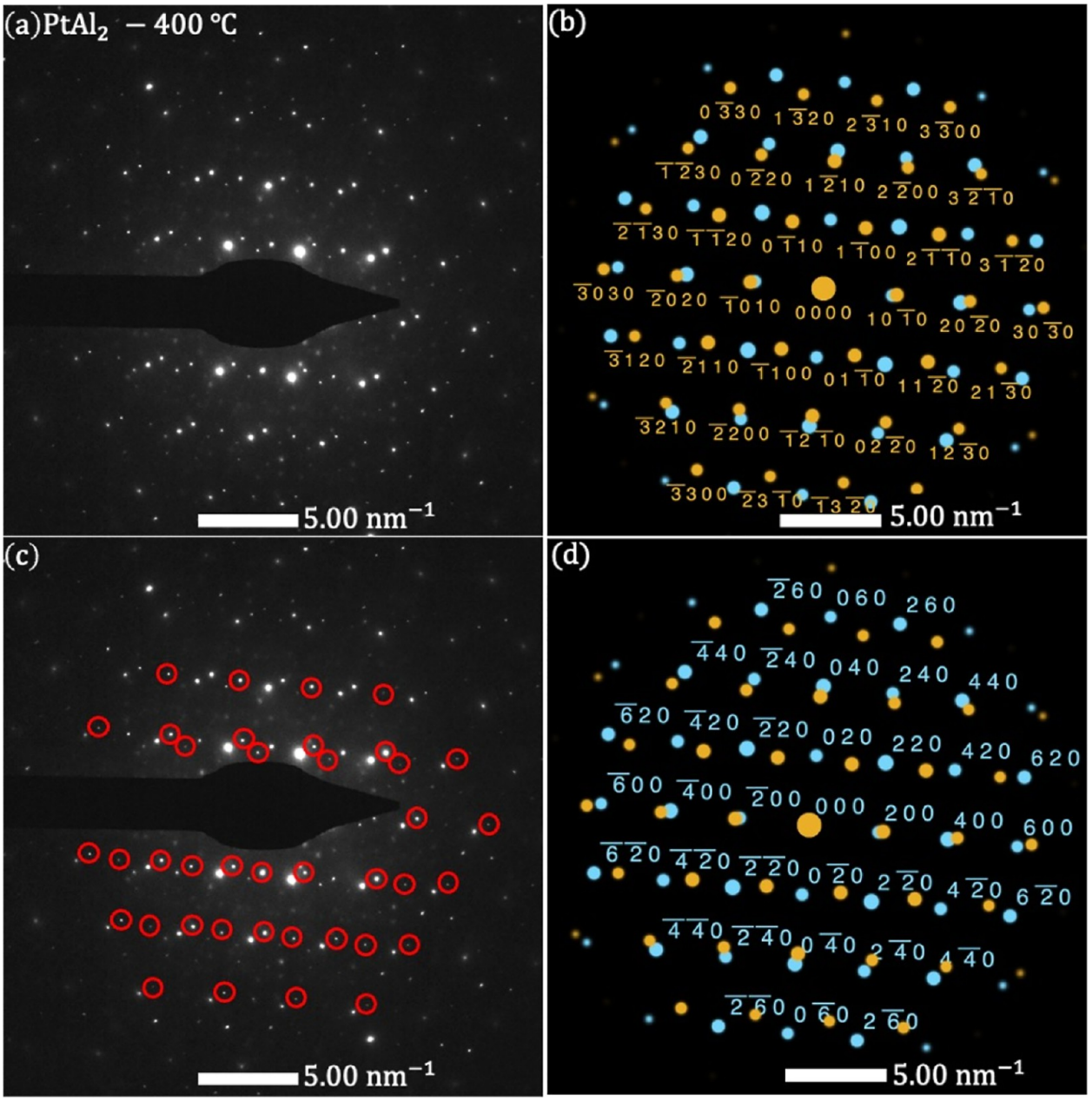

Figure 12. SAED pattern of $PtAl_2$ on MoS_2 (a) for the annealed condition (400 °C) and (b) simulated diffraction spots of the [100] zone axis of $PtAl_2$ with approximately 2° rotation relative to the [0001] zone axis of MoS_2 with the MoS_2 spots labeled. The orientational relationship is $PtAl_2$ (100)||MoS_2 (0001); $PtAl_2$ [0$\bar{2}$0]||MoS_2 [2$\bar{1}$$\bar{3}$0]. (c) SAED pattern showing double diffraction events circled. (d) Simulated diffraction spots of the [100] zone axis of $PtAl_2$ (labeled) with an approximately 2° rotation relative to the [0001] zone axis of MoS_2.

substrate stage at a temperature closer to but lower than the order−disorder transition could promote ordering.

4. CONCLUSIONS

We used our prior work on the quasi van der Waals epitaxy of elemental metals as a guideline to predict the low-temperature epitaxy of Pd and Pt-bearing intermetallics on MoS_2. We employed cosputtering to deposit PdCu, PtCu, PdIn, and $PtAl_2$, which are equilibrium ordered intermetallic phases at room temperature and also consistent with our criteria for low-temperature epitaxy. Our SAED patterns showed the formation of oriented but disordered PdCu on exfoliated MoS_2. Its orientation relationship matches other examples of the epitaxy of FCC metals on MoS_2. We were able to form ordered PtCu after annealing as well as highly textured PdIn films on MoS_2 at room temperature and after annealing, which matched our predictions. Additionally, we formed ordered $PtAl_2$ after annealing, but with the (100) plane and not the initially expected (111) plane on the (0001) MoS_2 surface. Overall, our study demonstrated the opportunities and challenges of using 2D materials as growth templates for single crystals of ordered intermetallic phases.

■ ASSOCIATED CONTENT

Supporting Information

The Supporting Information is available free of charge at https://pubs.acs.org/doi/10.1021/acs.cgd.3c01167.

https://doi.org/10.1021/acs.cgd.3c01167
Cryst. Growth Des. 2024, 24, 1578−1590

Transmission electron micrographs of intermetallic films on exfoliated MoS_2 as deposited and after annealing (PDF)

AUTHOR INFORMATION

Corresponding Author

Suzanne E. Mohney − *Department of Materials Science and Engineering, The Pennsylvania State University, University Park, Pennsylvania 16802, United States; Materials Research Institute, The Pennsylvania State University, University Park, Pennsylvania 16802, United States;* orcid.org/0000-0001-5649-7640; Email: mohney@psu.edu

Author

Ama D. Agyapong − *Department of Materials Science and Engineering, The Pennsylvania State University, University Park, Pennsylvania 16802, United States;* orcid.org/0000-0001-6481-241X

Complete contact information is available at: https://pubs.acs.org/10.1021/acs.cgd.3c01167

Notes

The authors declare no competing financial interest.

ACKNOWLEDGMENTS

This work was partially supported by the George H. Deike, Jr. Research Grant at Penn State. The authors are also grateful to The Pennsylvania State University Two-Dimensional Crystal Consortium—Materials Innovation Platform (2DCC-MIP) supported by NSF cooperative agreement DMR-2039351, and A.A. acknowledges the Alfred P. Sloan Foundation for additional support through the Sloan Minority Ph.D. (MPHD) Program.

REFERENCES

(1) Furukawa, S.; Komatsu, T. Intermetallic compounds: Promising inorganic materials for well-structured and electronically modified reaction environments for efficient catalysis. *ACS Catal.* **2017**, *7*, 735−765.

(2) Watanabe, M.; Tsurumi, K.; Mizukami, T.; Nakamura, T.; Stonehart, P. Activity and stability of ordered and disordered Co-Pt alloys for phosphoric acid fuel cells. *J. Electrochem. Soc.* **1994**, *141*, 2659−2668.

(3) Furukawa, S.; Ochi, K.; Luo, H.; Miyazaki, M.; Komatsu, T. Selective stereochemical catalysis controlled by specific atomic arrangement of ordered alloys. *ChemCatChem* **2015**, *7*, 3472−3479.

(4) Furukawa, S.; Takahashi, K.; Komatsu, T. Well-structured bimetallic surface capable of molecular recognition for chemoselective nitroarene hydrogenation. *Chem. Sci.* **2016**, *7*, 4476−4484.

(5) Furukawa, S.; Endo, M.; Komatsu, T. Bifunctional catalytic system effective for oxidative dehydrogenation of 1-butene and n-butane using Pd-based intermetallic compounds. *ACS Catal.* **2014**, *4*, 3533−3542.

(6) Pavlišič, A.; Jovanovič, P.; Šelih, V. S.; Šala, M.; Bele, M.; Dražić, G.; Arčon, I.; Hočevar, S.; Kokalj, A.; Hodnik, N.; Gaberšček, M. Atomically resolved dealloying of structurally ordered Pt nanoalloy as an oxygen reduction reaction electrocatalyst. *ACS Catal.* **2016**, *6*, 5530−5534.

(7) Armbrüster, M.; Kovnir, K.; Behrens, M.; Teschner, D.; Grin, Y.; Schlögl, R. Pd-Ga intermetallic compounds as highly selective semihydrogenation catalysts. *J. Am. Chem. Soc.* **2010**, *132*, 14745−14747.

(8) Yan, Y.; Du, J. S.; Gilroy, K. D.; Yang, D.; Xia, Y.; Zhang, H. Intermetallic Nanocrystals: Syntheses and Catalytic Applications. *Adv. Mater.* **2017**, *29*, 1605997.

(9) Furukawa, S.; Ozawa, K.; Komatsu, T. Preparation of alumina-supported intermetallic compounds. *RSC Adv.* **2013**, *3*, 23269−23277.

(10) Menezes, P. W.; Panda, C.; Garai, S.; Walter, C.; Guiet, A.; Driess, M. Structurally ordered intermetallic cobalt stannide nanocrystals for high-performance electrocatalytic overall water-splitting. *Angew. Chem., Int. Ed. Engl.* **2018**, *57*, 15237−15242.

(11) Wang, Y.; Kim, J. C.; Wu, R. J.; Martinez, J.; Song, X.; Yang, J.; Zhao, F.; Mkhoyan, A.; Jeong, H. Y.; Chhowalla, M. Van der Waals contacts between three-dimensional metals and two-dimensional semiconductors. *Nature* **2019**, *568*, 70−74.

(12) Budania, P.; Baine, P. T.; Montgomery, J. H.; McNeill, D. W.; Neil Mitchell, S.; Modreanu, M.; Hurley, P. K. Comparison between Scotch tape and gel-assisted mechanical exfoliation techniques for preparation of 2D transition metal dichalcogenide flakes. *Nano-Micro Lett.* **2017**, *12*, 970−973.

(13) Li, H.; Wu, J.; Yin, Z.; Zhang, H. Preparation and applications of mechanically exfoliated single-layer and multilayer MoS_2 and WSe_2 nanosheets. *Acc. Chem. Res.* **2014**, *47*, 1067−1075.

(14) Ooi, S. I.; Ahmad, H. Thermal release tape assisted mechanical exfoliation of pristine TMD and the performance of the exfoliated TMD saturable absorbers for Q-switched laser generation. *Opt. Mater.* **2022**, *128*, 112363.

(15) Huo, C.; Yan, Z.; Song, X.; Zeng, H. 2D materials via liquid exfoliation: a review on fabrication and applications. *Sci. Bull.* **2015**, *60*, 1994−2008.

(16) Jawaid, A.; Che, J.; Drummy, L. F.; Bultman, J.; Waite, A.; Hsiao, M.-S.; Vaia, R. A. Redox Exfoliation of Layered Transition Metal Dichalcogenides. *ACS Nano* **2017**, *11*, 635−646.

(17) King, L. A.; Zhao, W.; Chhowalla, M.; Riley, D. J.; Eda, G. Photoelectrochemical properties of chemically exfoliated MoS_2. *J. Mater. Chem. A* **2013**, *1*, 8935.

(18) Domask, A. C.; Cooley, K. A.; Kabius, B.; Abraham, M.; Mohney, S. E. Room Temperature van der Waals Epitaxy of Metal Thin Films on Molybdenum Disulfide. *Cryst. Growth Des.* **2018**, *18*, 3494−3501.

(19) Cooley, K. A.; Alsaadi, R.; Gurunathan, R. L.; Domask, A. C.; Kerstetter, L.; Saidi, W. A.; Mohney, S. E. Room-temperature epitaxy of metal thin films on tungsten diselenide. *J. Cryst. Growth* **2019**, *505*, 44−51.

(20) van der Lingen, E. Aspects of coloured precious metal intermetallic compounds. *J. South. Afr. Inst. Min. Metall.* **2014**, *114*, 137−144.

(21) Cui, C.-H.; Li, H.-H.; Liu, X.-J.; Gao, M.-R.; Yu, S.-H. Surface composition and lattice ordering-controlled activity and durability of CuPt electrocatalysts for oxygen reduction reaction. *ACS Catal.* **2012**, *2*, 916−924.

(22) Cai, X.; Wang, A.; Wang, J.; Wang, R.; Zhong, S.; Zhao, Y.; Wu, L.; Chen, J.; Bai, S. Order engineering on the lattice of intermetallic PdCu co-catalysts for boosting the photocatalytic conversion of CO_2 into CH_4. *J. Mater. Chem. A* **2018**, *6*, 17444−17456.

(23) Jain, A.; Ong, S. P.; Hautier, G.; Chen, W.; Richards, W. D.; Dacek, S.; Cholia, S.; Gunter, D.; Skinner, D.; Ceder, G.; Persson, K. A. Commentary: The Materials Project: a materials genome approach to accelerating materials innovation. *APL Mater.* **2013**, *1*, 011002.

(24) Li, M.; Du, Z.; Guo, C.; Li, C. A thermodynamic modeling of the Cu−Pd system. *Calphad* **2008**, *32*, 439−446.

(25) Abe, T.; Sundman, B.; Onodera, H. Thermodynamic assessment of the Cu−Pt system. *J. Phase Equilibria Diffus.* **2006**, *27*, 5−13.

(26) Okamoto, H. In-Pd (Indium-Palladium). *J. Phase Equilib.* **2003**, *24*, 481.

(27) Wu, K.; Jin, Z. Thermodynamic assessment of the Al-Pt binary system. *J. Phase Equilib.* **2000**, *21*, 221−226.

(28) Saidi, W. A. Trends in the Adsorption and Growth Morphology of Metals on the MoS_2(001) Surface. *Cryst. Growth Des.* **2015**, *15*, 3190−3200.

(29) Domask, A. C.; Gurunathan, R. L.; Mohney, S. E. Transition metal−MoS_2 reactions: review and thermodynamic predictions. *J. Electron. Mater.* **2015**, *44*, 4065−4079.
(30) Yuan, F. T.; Huang, H. W.; Liao, W.; Chang, H. W.; Sun, A. C.; Hsiao, S.; Chen, S. K.; Lee, H. Y. Tetragonal-to-cubic transformation of CoPt in post-annealed CoPt and CoPt/Au thin films. *IEEE Trans. Magn.* **2009**, *45*, 2682−2685.
(31) Okamoto, H. Co-Pt (Cobalt-Platinum). *J. Phase Equilib.* **2001**, *22*, 591.

https://doi.org/10.1021/acs.cgd.3c01167
Cryst. Growth Des. 2024, 24, 1578−1590